Premelting at ice-solid interfaces studied via velocity-dependent indentation with force microscope tips

B. Pittenger, S. C. Fain, Jr.,* M. J. Cochran, J. M. K. Donev, B. E. Robertson, A. Szuchmacher, and R. M. Overney
University of Washington, Seattle, Washington 98195-1560

(Received 29 June 2000; revised manuscript received 28 September 2000; published 2 March 2001)

We have indented the surface of ice at temperatures between −1 °C and −17 °C with sharp atomic force microscope tips. For a thick viscous interfacial melt layer, a Newtonian treatment of the flow of quasiliquid between the tip and the ice suggests that indentations at different indentation velocities should have the same force/velocity ratio for a given pit depth. This is observed for silicon tips with and without a hydrophobic coating at temperatures between −1 °C and −10 °C implying the presence of a liquid-like layer at the interface between tip and ice. At temperatures below about −10 °C the dependence of force on velocity is weaker, suggesting that plastic flow of the ice dominates. A simple model for viscous flow that incorporates the approximate shape of our tip is used to obtain an estimate of the layer thickness, assuming the layer has the viscosity of supercooled water. The largest layer thicknesses inferred from this model are too thin to be described by continuum mechanics, but the model fits the data well. This suggests that the viscosity of the confined quasiliquid is much greater than that of bulk supercooled water. The hydrophobically coated tip has a significantly thinner layer than the uncoated tip, but the dependence of thickness on temperature is similar. The estimated viscous layer thickness increases with increasing temperature as expected for a quasiliquid premelt layer.

DOI: 10.1103/PhysRevB.63.134102 PACS number(s): 64.70.Dv, 83.50.Lh, 62.20.Qp, 83.10.Gr

I. INTRODUCTION

Slightly below the melting point a thin liquidlike layer exists at the interface between ice and some materials.[1,2] This interfacial premelt layer or quasiliquid layer (QLL) has been most often studied in the case of the ice-vapor interface,[3–8] but premelting can also occur at ice-solid interfaces. The properties of this layer depend on the other solid at the interface, on the presence of impurities and on the temperature.

Because ice-solid interfaces are very common on our planet, knowledge of the properties of the ice-solid QLL are important to understand many environmental processes. The presence of a QLL can decrease the friction between solids and ice. This has been suggested as a source of lubrication in the sliding of glaciers[9] and iceskates.[10] Additionally, the adhesion of ice to solids, such as airplane wings and windshields, may be influenced by the QLL.[11] Finally, the QLL can allow water to be efficiently transported at temperatures below melting. This process can weather rock and break up roadways through frost heave.[1] The relative importance of the QLL in each of these processes depends on the properties of the quasiliquid (such as thickness and viscosity) in the environment of interest and on any other mechanisms that are present.

Figure 1 shows the thickness of the QLL as a function of temperature for several experiments at both ice-QLL-solid[12–15] and ice-QLL-vapor[6,16–18] interfaces. The variation in thickness data is not surprising, since the properties of the QLL are expected to depend on the chemical and physical properties of the other material at the interface, the crystallinity and orientation of the ice, and impurities present in the ice and interfacial region.[19–21] Additionally, it is not clear that all measurements of the QLL thickness are really measuring the same physical property. Dynamic measurements, such as pushing ice cylinders through quartz capillaries,[22–24] pulling wires through ice blocks,[12] sliding friction measurements,[25] and measurements of the deformation of an elastic film in contact with ice in a temperature gradient[14] are sensitive to the viscosity of the layer to varying extents. Ellipsometry[19] and nuclear magnetic resonance[15] measurements depend on other properties of the quasiliquid. The viscous layer may not extend into the ice the same distance as the other interfacial properties, such as disorder and index of refraction, so care must be used in comparing thicknesses obtained with techniques that are sensitive to the viscosity of the quasiliquid to those that are not.

In this paper, we will discuss various mechanisms that can produce indentations in ice and present data suggesting that a viscous layer is present between the tip and the ice for high enough temperatures and some tip materials. We will discuss a model that, given the viscosity of the layer, allows us to estimate its thickness. While the data analyzed for this paper are taken under dynamical conditions, the QLL is expected to be near thermal equilibrium, since the heat required to form the QLL can be rapidly provided from the environment around the indentation.[26]

II. EXPERIMENT

The data described in this paper were collected with a home-built atomic force microscope (AFM), custom designed to minimize drift and stabilize the thickness of the ice sample.[27,28] Since our last report,[29] a dry box has been added around the cooled portions of the microscope in order to decrease temperature gradients around the sample due to convection and to stop water from condensing on the optics. Also, the electronics have been upgraded for faster response

 ©2001 The American Physical Society

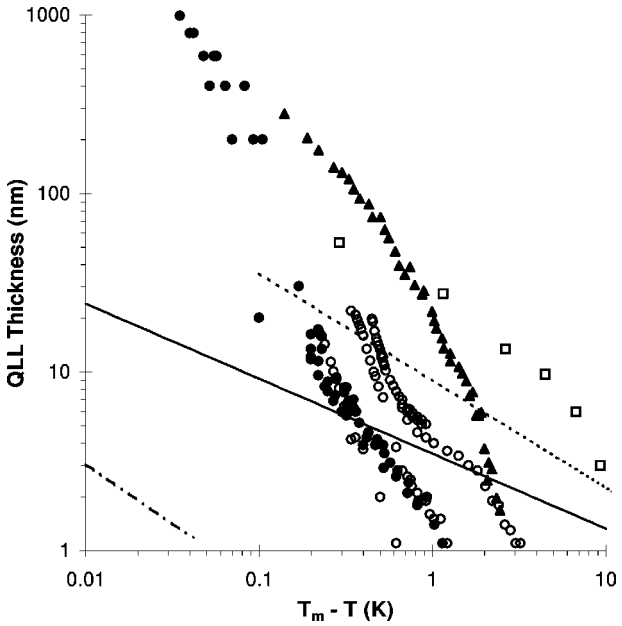

FIG. 1. Interfacial quasiliquid layer thickness as a function of temperature below melting. The dot-dashed line is a fit of the thicknesses obtained for an ice-polymer interface from flow of the layer under the influence of a temperature gradient assuming the layer has the viscosity of supercooled water (Refs. 13 and 14). The solid line is a fit of the thicknesses obtained for ice-metal interfaces from wire regelation experiments assuming the layer has the viscosity of supercooled water (Ref. 12). The dashed line is for ice-glass interfaces as measured with NMR (Ref. 15). Circles are thicknesses obtained using optical reflectivity (Refs. 6 and 16): filled circles are for the ice (0001)-air interface, open circles are for the (0001)-vapor interface. Filled triangles are the result using ellipsometry to find the thickness at the ice (0001)-air interface (Ref. 17). Open squares are for the ice (0001)-vapor interface studied with glancing x-ray scattering (Ref. 18).

and to allow photodiode signal gain control. Finally, an optical microscope has been incorporated for observation of the ice and tip at scales greater than a few tens of microns.

A fresh, polycrystalline ice sample is prepared for each data run (for each tip). With the sample chamber pumped down to less than 0.002 Torr, the gold-plated sample substrate is cooled to less than $-20\,^{\circ}\mathrm{C}$. Triply distilled, deionized, and degassed water vapor is then dosed into the sample chamber until there is enough water present to cover the sample substrate with a layer of ice about 0.5 mm thick.[30] This process typically takes about 30 min. Because the sample substrate is the coldest point in the sample chamber, the water vapor rapidly moves there. After dosing, we wait at least an hour before taking data to allow the ice to equilibrate. At that point, the ice appears smooth at the scale that is visible in our optical microscope.

The properties of the ice surface are highly dependent on any impurities that are present.[21] The main potential sources of contamination of the ice include the tip, the sample substrate, and the surrounding gases. In the experiments described here there is less than 0.1 Torr of atmospheric gases present (this small amount is due to leakage of the chamber during the data run). If the growing ice originates under the layer of contaminants on the sample substrate, this layer could be pushed to the surface during growth. In order to minimize the possibility of this, we have carefully cleaned the substrate with methanol and acetone, dried it with nitrogen, and stored it under vacuum. At this time, we have not found a good way to clean our tips, so the tip may be the primary source of impurities on our ice surfaces.[31]

In order to keep ice from condensing on the tip and cantilever (where it would change the spring constant and tip geometry), the tip is kept slightly warmer than the ice. This is accomplished by using a Peltier cooler to control the temperature of a thermistor located in the cantilever mount, about 1 mm from the cantilever. This temperature was kept about $0.1\,^{\circ}\mathrm{C}$ warmer than the sample substrate. The temperature difference between the tip and sample depends on the contact area of the tip on the ice. If the tip is far from the ice surface, the incident laser power (kept at a constant level of less than 25 μW during each experiment), which is conducted back through the cantilever to the mount, causes the tip temperature to be about $0.3\,^{\circ}\mathrm{C}$ warmer than the ice substrate. If the tip is indented into the ice by 25 nm, some of the heat from the laser can be conducted into the ice, and the tip is estimated (using the method of Eastman and Zhu[32]) to be only $0.1\,^{\circ}\mathrm{C}$ warmer than the substrate. Deeper indentations will decrease the temperature difference by increasing the tip-ice contact area.

Once the ice has equilibrated and the tip temperature is lowered to a temperature slightly warmer than the ice, we begin taking data. By collecting *force curves* we can study the normal forces between the tip and sample as a function of sample position, speed, and temperature. To collect a force curve, the sample is moved toward the tip (approach) and then away from the tip (retract), while the position of the laser spot on the photodiode is measured (Fig. 2). The whole process can take as little as 34 ms for the curves collected at the fastest sample rates or as long as 8 s for the slowest. Initially, there is no deflection of the cantilever because the tip-sample separation is greater than the range of tip-sample forces (point *A*). At point *B*, the gradient of the tip-sample force becomes greater than the spring constant of the cantilever, and the tip suddenly jumps to the surface (*jump-in* or *jump-to-contact*).[33] The tip then stays in contact with the surface as the sample is moved toward the tip and the measured force changes from attractive to repulsive. Eventually, the *maximum measured force* is reached at point *C*.[34] The sample is then moved away from the tip, but the measured force is still repulsive until point *D*. The distance from the origin to point *D* is roughly the maximum indentation depth. At point *E* the tip-sample force gradient becomes greater than the spring constant of the cantilever, and the tip jumps free of the surface (*pull-off*).

A. Instrumental calibration

Quantitative measurement in AFM requires calibration of sample position (Z_s) and cantilever deflection (Z_c) as a function of signals from the control electronics. In addition, the normal spring constant (K) of the cantilever is needed to convert the cantilever deflection into measured force using

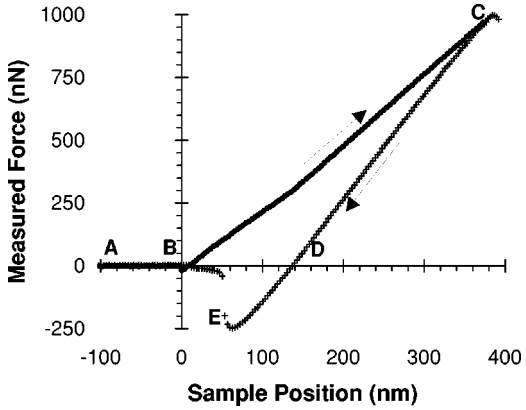

FIG. 2. A typical force curve collected at −10.9 °C in pure water vapor with a coated tip (tip *C*). The upper points (filled circles) are the approach data; the lower points (plus signs) are the retract data. The whole curve was collected in 34 ms. The curve has been shifted so that the first deviation from zero force (the *jump-in* at *B*) occurs at a sample position of zero. The calibration procedure described in the text causes the retract curve from *C* to *D* to have a slope approximately equal to the spring constant.

$F=KZ_c$. Finally, we must know the geometry of the end of the tip in order to quantify the indentation process.

The sample position as a function of applied voltage, scan range, acquisition time, and temperature of the piezoelectric positioner (piezo) is obtained using interference fringes during special calibration measurements.[30] Interference between laser light reflected from the back of a cantilever and that reflected from a special mirrored sample results in a roughly sinusoidal signal at the photodiode, when force curves are collected without contacting the sample. This allows us to obtain a calibration of the sample position that corrects for the effects of piezo creep, hysteresis, and nonlinearity which are present to some extent in all piezoelectric positioners.[35] Using our single tube piezo additional calibrations would be required for each lateral position. Therefore, all of the indentation data reported here was taken with lateral offsets of zero volts. This does not mean that all of the data was collected at precisely the same point on the sample, since each approach lands the tip at a slightly different position, but that position probably varied less than 0.5 μm.

The cantilever deflection calibration is obtained by averaging the retract slopes of the fastest force curves at the lowest possible temperatures. Assuming creep and other time dependent processes can be neglected in these fast curves, the shape of the retract curve is determined by the elastic properties of the ice and the tip, not their plastic properties.[36] Because the cantilever is much less stiff than the ice surface, the elastic deformation of the ice may be neglected in comparison to the deflection of the cantilever, and the change in deflection of the cantilever approximately equals the change in sample position ($dZ_c/dZ_s \approx 1$). The calibration procedure causes the retract curve in Fig. 2 to have a slope approximately equal to the spring constant. This calibration is sensitive to the position and shape of the laser spot on the cantilever, so if the laser spot moves over the course of an experiment the calibration must be acquired once again.

TABLE I. Properties of tips and cantilevers used in these experiments.

Tip	Batch	K (N/m)	R (nm)	α (°)	Coated?
A	006–014	0.85±0.30	25±8	14±3	No
B	017–043	4.1±1.4	19±5	11±2	No
C	017–043	4.6±1.6	25±10	15±3	Yes

Slight changes in calibration were tracked by periodically moving the photodiode a known amount and recording the change in signal recorded by the AFM, with the tip far from contact.[37]

B. Cantilever characterization

As previously stated, the spring constant of the cantilever must be known in addition to the deflection to determine the measured force. If the geometry and elastic constants of the cantilever are known, the spring constant may be roughly calculated. Typically, the largest uncertainty in this sort of calculation arises from the measurement of the thickness of the cantilever or variation in elastic constants due to unknown stoichiometry of the cantilever material (e.g., silicon nitride). Boron-doped silicon cantilevers, such as ours,[38] have well-known elastic constants and are conductive enough to be imaged in a field emission scanning electron microscope (SEM) for measurement of their thickness. The spring constants given in Table I were calculated using the analytical method of Neumeister and Ducker.[39] The uncertainty in the spring constants is about 30%, and is mainly due to poor knowledge of the calibration of the SEM. Three cantilevers were used to obtain the data reported in this paper (see Table I). Cantilevers *A* and *B* are uncoated cantilevers with normal spring constants of 0.85 N/m and 4.1 N/m, respectively. Some of the data collected with cantilever *A* was previously reported.[29] Cantilever *C* is hydrophobically coated with a spring constant of 4.6 N/m. The hydrophobic coating is far too thin to influence the spring constant significantly.

A simple approximation of the tip profile is a cone truncated in a portion of a sphere. With this approximation, the radius of the truncating sphere (R) and the half-angle of the cone (α) parameterize the radius (g) of a cross section of the tip, where the distance from the end of the tip (ζ) is measured along its axis of symmetry:

$$g(\zeta)=R\begin{cases}\sqrt{2\dfrac{\zeta}{R}-\left(\dfrac{\zeta}{R}\right)^2} & \text{if } \dfrac{\zeta}{R}\leqslant 1-\sin\alpha,\\ \sec\alpha+\left(\dfrac{\zeta}{R}-1\right)\tan\alpha & \text{otherwise.}\end{cases} \quad (1)$$

The end radius and cone half angle of the tip are measured using field emission SEM. This provides reasonably accurate dimensions for the silicon tips, but removes any hydrophobic coating before its thickness may be measured. The thickness of these coatings must be estimated from x-ray photoelectron spectroscopy (XPS) measurements of flat films from the

same batch. The dimensions for tip *C* given in Table I include the estimated coating thickness as discussed below.

The hydrophobic coating was made by reacting octadecyltrichlorosilane with the native oxide present on the silicon cantilever.[40] Water droplets on flat surfaces treated with this technique have typical contact angles of about 105° compared to 55° for flat silicon surfaces with native oxide or 80° for glass surfaces stored in a manner similar to our tips.[31] XPS measurements of flat surfaces coated along with the cantilever indicated film thicknesses of 4–8 nm. AFM measurements of these films on flat surfaces showed that 5%–10% of the surface area had bumps 5–10 nm high. A 10 nm thick coating increases the tip radius from 15 nm (as measured in field emission SEM) to roughly 25 nm. The bumps will alter the geometry of the tip slightly, but the tip profile given by Eq. (1) will still give the approximate tip shape. Prolonged imaging of the flat films with contact AFM did not damage the films to any noticeable extent, suggesting that the films are quite durable. There is no guarantee that the coating on the tip will be identical to that on the flat surface, but we have yet to find a better way to determine the properties of the coating on tips as sharp as these.

III. RESULTS

To obtain information about the mechanical properties of the ice-tip interface, we collected force curves at several temperatures and sample speeds for each tip. Once the instrument has been calibrated, the force curves can be converted to force versus indentation curves since the deflection of the cantilever (Z_c) and the sample position (Z_s) are both known. If the arbitrary offset in the sample position is chosen so that $Z_s=0$ at the first point during the approach where $Z_c\neq 0$ (as shown in Fig. 2), then the indentation depth (z) is given by $z=Z_s-(Z_c-Z_c|_{Z_s=0})$. This assumes that the tip has come into contact with the surface, but there has not yet been any indentation at $Z_s=0$. In the experiments described here, $Z_c|_{Z_s=0}$ is less than 5 nm, as discussed in more detail below, so it can be neglected for larger indentation depths. The indentations deduced are expected to be accurate within a few percent except at the smallest depths. The force can then be plotted against the indentation depth instead of the sample position, as shown in Fig. 3. Note that the maximum indentation depth in Fig. 3 is approximately equal to the change in sample position from *B* to *D* in Fig. 2.

After the jump-in, the measured force versus indentation curve gives the force required to obtain a given indentation depth (neglecting attractive forces such as those responsible for the jump-in). With our experimental parameters, it is easy to indent the ice by hundreds of nanometers. The first few points after the jump-in in Fig. 3 have positive indentation depths, despite the negative measured force. Adhesive forces between the tip and the sample increase the total force on the ice under the tip to the point where the ice surface can be indented. As the indentation depth increases, more externally applied force is required to increase the indentation, and the adhesive forces between the tip and the ice become small compared to the measured force.

At the beginning of the retraction portion of the curve (while the measured force is positive), there is little change in the indentation depth. This is not surprising due to our technique for calibrating the cantilever deflection. If there is noticeable additional indentation, it is expected to result from creep or viscous flow, not from instantaneous plastic flow or elastic deformation. When the measured force becomes negative, there may be some instantaneous plastic flow, creep, or viscous flow in the opposite direction. This occurs in Fig. 3 in the region near the minimum in measured force.

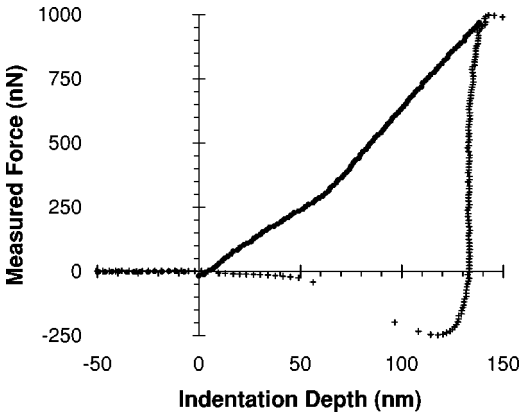

FIG. 3. Measured force versus indentation depth curve collected at −10.9 °C in 34 ms with tip *C* (data from Fig. 2 plotted versus indentation depth instead of sample position). The upper points (filled circles) are the approach data; the lower points (plus signs) are the retract data. For this data the indentation speed at 100 nm depth is approximately 15 μm/s.

After the tip breaks free of the surface, the depression fills in after a few seconds out of contact due to vapor transport to the region of negative curvature (from the Kelvin equation, the depression has a lower vapor pressure than the surrounding flat surface[41]). If the pit did not fill in from one indentation to the next or the geometry of the surface changed significantly in any way, we would expect the force curves to change as well. In fact, we observe only small variations in repeated force curves taken with all the same parameters, except the time since the last tip contact to the surface.

A. Indentations at different velocities

In order to distinguish between the different mechanisms by which a deformation can form, we have collected force curves at different sample velocities. Although indentations are sometimes conducted at a constant ''indentation strain rate,'' [42] the constant sample velocity at which each approach curve is collected in our experiments does not result in a fixed strain rate. Instead, the changing size and shape of the indentation and the bending of the cantilever cause the stress on the ice to vary as the sample is moved. This, in turn, causes the indentation velocity to change as a function of sample position. Given the indentation depth (z) and time (t) at adjacent data points, we can find the indentation velocity ($v=\Delta z/\Delta t$) as a function of indentation depth.

Figure 4 gives the approach curves for several indentations with the coated tip (*C*) at −5.3 °C and various sample velocities. The indentation velocities given are for indenta-

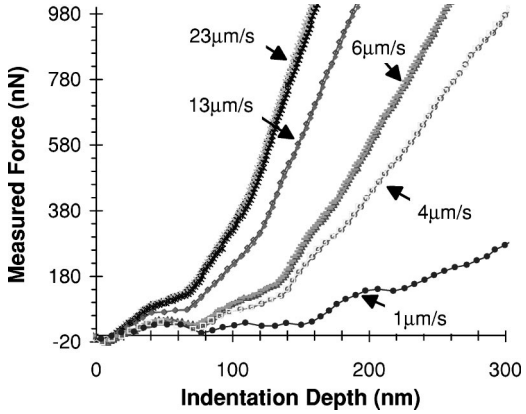

FIG. 4. Measured force versus indentation depth at −5.3 °C and several sample velocities collected with (coated) tip *C*. The approximate indentation velocity at an indentation depth of 100 nm is given for each curve. Only the approach portion of each curve is shown.

tion depths of 100 nm. Two curves are shown at each sample velocity (except 1 μm/s) to illustrate the consistency of the results. To obtain similar indentation depths with an uncoated tip (*B*), significantly less force is required. For both tips, much more force is required to get the same indentation depth for the faster speeds than for the slower speeds. This is especially true at temperatures above −10 °C where a QLL might play a role.

In addition to the expected smooth monotonic increase in force required to increase the indentation depth, we often observe inflection points or dips in the force during the contact portion of the curve (see Fig. 4). These dips occur at about the same indentation depth independent of sample speed and temperature, as opposed to the same force as would be expected for a process that occurs at a threshold force. For example, Fig. 4 and the curve in Fig. 3 at −5.3 °C both show a dip near 60 nm indentation depth. Dips in the slower curves at −5.3 °C are more evident in Fig. 5 where the logarithmic scales combined with dividing the smaller forces by the smaller speeds makes the dips more obvious. The presence of the dips at the same indentation depth is

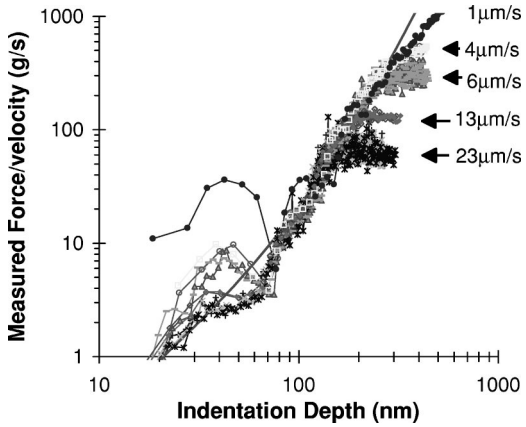

FIG. 5. Measured force divided by indentation velocity versus indentation depth at −5.3 °C and several sample velocities collected with tip *C* (data from Fig. 4). The line without point markers is a fit to the data using the viscous model discussed in Sec. IV D below.

consistent with the possibility that the dips are caused by chemical heterogeneities (due to the bumps of hydrocarbon that formed on the tip during coating) which produce variations in total force at the same measured force. As mentioned earlier, bumps 5–10 nm high were observed on the flat coated along with tip *C*. The changes in force responsible for the dips seem to be roughly independent of speed, but at the highest speeds the dips in force are small compared to the measured force, making them less obvious. This implies that variations in tip surface chemistry with indentation depth are primarily responsible for the dips, since deviations from the simple sphere-cone tip geometry should result in larger variations in force for the faster curves. The data collected with the coated tip (*C*) have larger dips than the data collected with the uncoated tips (not shown here, but available elsewhere[30]), suggesting that the uncoated tips are smoother and less chemically heterogeneous than the coated tip.

When an indentation is formed, water molecules are moved from under the tip to the surface of the ice. In plastic flow, the water remains solid during this process. In the presence of a viscous layer between the tip and the ice, a second mechanism can occur. The viscous layer can flow to the surface, transporting the water molecules and increasing the size of the indentation. If additional ice is converted to quasiliquid in such a way as to keep the thickness of the layer constant during the indentation, then we might expect the force required to expel it from under the tip to be proportional to the indentation velocity. This is demonstrated in Sec. IV D below. Plotting the ratio of the force to the velocity against the indentation depth should, therefore, cause all of the curves in Fig. 4 to collapse onto one curve.

Figure 5 shows the ratio of the force to the velocity as a function of indentation depth at −5.3 °C for data collected with the coated tip (*C*). From an indentation depth of 70 nm to about 200 nm, the curves have about the same ratio of force to velocity at a given indentation depth. Data collected with the uncoated tip (*B*) (not shown here, but available elsewhere[30]) also has a region where all but the slowest curves agree at −5.3 °C. The region of agreement for the uncoated tip extends from indentation depths of about 100 nm to about 300 nm. For both tips, the force/velocity ratio levels off at large indentation depths and the force is no longer proportional to the velocity. This occurs at smaller indentation depths for the faster curves. At small indentation depths, there is also disagreement between the ratios of force to velocity for different speeds. In this case, the slower curves require larger force/velocity ratios than the faster curves at the same indentation depth. Forces between the tip and ice caused by attractive capillary forces[43] or repulsive disjoining pressure[44] may cause this disagreement, since they do not scale with indentation velocity and are not included in the measured force, but they do play a role in the indentation process. Because the measured force is smaller for the slower curves, these forces will be larger in comparison, causing disagreement between the curves collected at different speeds.

Similar plots at −3 °C give similar results for both tips, but force/velocity data collected at −15 °C (Fig. 6) and −17 °C does not collapse onto one curve as well as the data

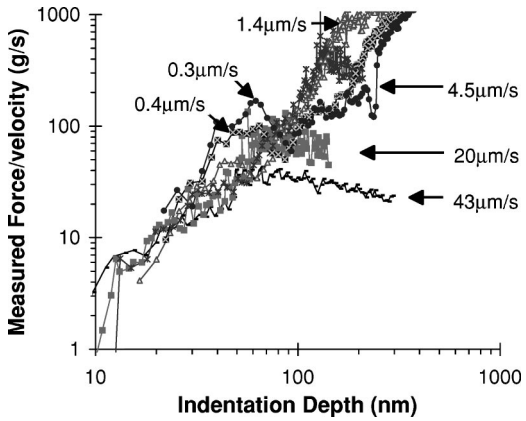

FIG. 6. Measured force divided by indentation velocity versus indentation depth at −15.1 °C and several sample velocities collected with tip *C*. The approximate indentation velocity at an indentation depth of 100 nm is given for each curve. Only the approach portion of each curve is shown.

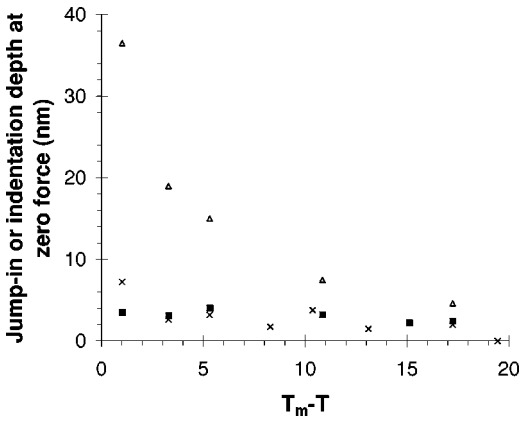

FIG. 7. Average jump-in distance measured with tip *B* (crosses) and tip *C* (filled squares) as a function of temperature below melting. Open triangles are the average indentation depth at zero measured force collected with tip *C*. Only curves collected at acquisition rates of greater than 500 samples/s were included in the averages.

at higher temperatures. Instead, the ratio of force to velocity depends upon the sample speed as well as the indentation depth. This is because there is not as much variation in the force with indentation velocity at low temperatures as there is at the higher temperatures where a QLL is expected to have significant thickness. As expected, significantly more force is required to form an indentation at lower temperatures at a given velocity than is required near the melting point. This is illustrated by comparing Figs. 5 and 6—the ratio of force to velocity is about a factor of 10 larger at −15 °C than it is at −5 °C at a given indentation depth.

B. Cantilever instabilities

It has long been known that the competition between tip-sample forces and the force on the tip due to the bending of the cantilever can cause instabilities in the tip position.[33] These instabilities typically occur when the force gradient between the tip and the sample exceeds the spring constant of the cantilever on approach (jump-in) or retract (pull-off). They are characterized by a change in tip position (measured force) which occurs in a time on the order of the resonant period of the cantilever, since the actual force changes much more rapidly than this time (for most cantilevers). The resonant frequencies of our cantilevers were over 50 KHz and our maximum sample rate is 15 000 samples/s (the bandwidth of our electronics is about 20 KHz), so instabilities show up as abrupt steps in the force curve (such as at point *E* in Fig. 2).

When the tip first contacts the surface during an approach, a jump-in will sometimes occur. Whether there is a jump, and the distance from the surface at which it occurs, is determined by the spring constant of the cantilever and the force gradient that the sample exerts on the tip before the tip comes into contact with a solid surface. Any attractive force (e.g., van der Waals, electrostatic, or capillary) can produce a jump-in if the spring constant of the cantilever is weak enough. In particular, capillary forces often dominate in situations where water vapor is present (and the temperature is above 0 °C).[43] For a hydrophobic tip one might expect that the capillary force would be repulsive, excluding capillary forces as the cause of a jump-in. Actually, the capillary forces can pull the tip in for contact angles (for the liquid on the tip, the liquid is assumed to wet the sample) up to $\alpha + 90°$ for a meniscus that meets the tip in the conical region (where α is the half-angle of the cone). The capillary force can remain attractive for even larger contact angles if the meniscus meets the tip in the hemispherical region.[45]

Previous authors have used the jump-in distance to estimate the thickness of liquid layers on surfaces.[26,45–48] However, the thickness of this layer is not necessarily given by the jump-in distance. The jump-in may occur before the tip contacts the liquid layer due to condensation in the region between the tip and the layer, or due to deformation of quasiliquid up to meet the tip. In addition, the tip may not stop precisely at the solid surface when it is pulled in by the attractive forces. Depending on the spring constant of the cantilever and the force from the meniscus, it may find mechanical equilibrium in the liquid layer, or may significantly indent the ice before the next data point can be collected. In spite of this, some investigators have claimed that the jump-in may provide a way to probe the ice-vapor interface instead of the ice-tip interface that is probed by most of the rest of the force curve.[26,45,47,48] Figure 7 gives the jump-in distance ($-Z_c|_{Z_s=0}$) averaged over many measurements as a function of temperature for tips *B* and *C*. The jump-in distances are roughly the same for both tips and are approximately constant (≈3 nm) with temperature. Since the jump-in distances that we measure are roughly independent of temperature, it seems unlikely that the thickness of the ice-vapor QLL is directly related to the jump-in distance.

For comparison to the jump-in distance, the indentation depth at the point where the measured force again becomes zero after the jump-in ($z|_{Z_c=0}$) is also given in Fig. 7 for the coated tip (*C*). While the jump-in distance is roughly constant with temperature in our measurements, there is significant increase in indentation depth (at zero measured force)

due to tip-sample attractive forces. Although the attractive forces may change slightly with temperature, the increase in indentation depth is primarily due to the decrease in the force required to indent the ice as the temperature increases. This increase in indentation due to attractive forces may explain the results of Döppenschmidt *et al.*[45,48] who observed much larger jump-in distances than ours and significant variation with temperature. The relatively compliant cantilevers that they used may have allowed the attractive forces to indent the ice between the collection of adjacent data points in the force curve, causing the observed temperature dependence and increased jump-in distances.

When the tip breaks free of the ice, the break may occur at the tip-ice interface or somewhere in the ice.[49] If the spring constant is large and the ice is soft (or the tip-ice interface is strong), the process of separation may be drawn out over hundreds of nanometers, and there may be no distinct pull-off. As a result, it may be difficult to interpret what the pull-off force means. With tips *B* and *C* we typically saw increasing pull-off forces for larger maximum measured forces (larger indentations), but the pull-off forces were usually smaller than the maximum measured forces. This is in contrast to the results of our previous paper[29] where the pull-off forces were approximately equal to the maximum measured forces suggesting that (with tip *A*) the ice was breaking instead of the ice–solid interface. The more recent data collected with tips *B* and *C* suggest that the ice–ice bonding is stronger than the ice-tip bonding at those interfaces.

IV. DISCUSSION

The presence of the AFM tip in contact with the ice surface causes the ice to indent. There are several mechanisms by which this indentation can occur. In elastic deformation, the shape of the ice surface depends on the force on the tip, but not on the history of loading. Plastic deformation, on the other hand, involves pushing solid ice to the surface, leaving a pit that exists for a time after the tip is removed. Ice can also be deformed by converting some of the ice to liquid by pressure melting or interfacial premelting and squeezing this viscous layer between the tip and the remaining ice until it flows to the surface. To distinguish between the mechanisms by which the ice is deformed in our experiments, we must find the relationship between the force measured during the indentation and the indentation velocity for each mechanism.

A. Elastic deformation

There will be some elastic deformation of the ice under the tip.[29] The amount of elastic deformation is independent of time and loading history, but depends on the Young's modulus of the tip (E_{Si}) and ice (E_{ice}), the Poisson's ratios (ν_{Si} and ν_{ice}), the geometry of the tip-ice interface (approximated by the tip end-radius, R), and the force on the tip. For typical values ($E_{\mathrm{Si}}=160\,\mathrm{GPa}$ and $\nu_{\mathrm{Si}}=0.22$,[50] $E_{\mathrm{ice}}=9.4\,\mathrm{GPa}$ and $\nu_{\mathrm{ice}}=0.33$,[51] and $R=20\,\mathrm{nm}$) Hertzian mechanics gives an elastic deformation depth of 7 nm for a force of 1000 nN. Inclusion of attractive forces, as in the Johnson-Kendall-Roberts theory,[52] will increase the deformation depth by less than one nanometer at these high loads. The minimum deformation that we observe for measured forces similar to this is around 90 nm at $-15\,^{\circ}\mathrm{C}$, so elastic deformation may be neglected in comparison to the other deformation mechanisms.

B. Plastic flow

Uniaxial time dependent deformation of bulk ice at low enough strain rates and high enough temperatures has often[53–55] been described by empirical equations of the form:

$$\dot{\epsilon}=\sigma^{n}A\exp\left(-\frac{Q}{RT}\right), \tag{2}$$

where $\dot{\epsilon}$ is the strain rate, σ is the stress, A is a constant, Q is an activation energy, R is the gas constant, and T is the temperature. This is known as power-law creep, and involves both glide and climb of dislocations moving through the ice. For polycrystalline ice at low stresses, the exponent n is observed to be about three, but it increases rapidly for uniaxial stresses above about 1 MPa.[54] In order to compare the Meyer hardness ($H=F/A$, where F is the force and A is the projected area of the indentation) obtained at a given indentation strain rate ($\dot{\epsilon}_I=v/z$) from our indentation measurements to these uniaxial creep results, we will parallel the derivation of Poisl *et al.*[56]

Because our tip is sharp and the ratio of yield stress to elastic modulus of the ice is small, our indentations take place in the ''fully plastic'' regime.[29] The hardness in this regime is related to the uniaxial yield stress by[36,52]

$$H\approx 3\sigma. \tag{3}$$

The indentation strain rate can also be related to its uniaxial counterpart:[57]

$$\dot{\epsilon}=D\dot{\epsilon}_I, \tag{4}$$

where D is a constant. Combining Eqs. (2)–(4) and solving for hardness we find that

$$H\approx\dot{\epsilon}_I^{1/n}B\exp\left(\frac{Q}{nRT}\right), \tag{5}$$

where $B=3(D/A)^{1/n}$.

If the material displaced during plastic indentation is assumed to be carried off by vapor transport, surface diffusion or flow of the ice-vapor QLL, effects such as ''pile-up'' and ''sink-in'' that deform the ice-vapor interface[36] can be neglected. The contact radius at indentation depth z is then just the radius of the cross section of the tip at the proper distance from the end of the tip, $g(\zeta=z)$. To first approximation, the Meyer hardness of the ice is then simply related to the measured force required to obtain a given indentation depth, the indentation strain rate, and the indentation depth:[58]

$$H(\dot{\epsilon}_I)\approx\frac{F(z,\dot{\epsilon}_I)}{\pi g(z)^2}. \tag{6}$$

This equation is approximate because the contact area is probably not precisely given by the cross-sectional area of

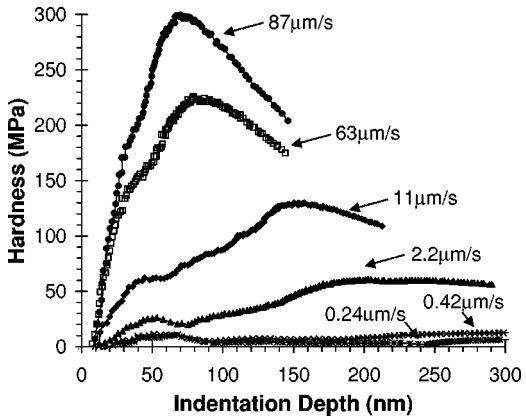

FIG. 8. Measured hardness [from Eq. (6)] versus indentation at −15.1 °C collected with tip *C* at various sample velocities. Only the approach data is shown. For bulk ice, pressure melting at this temperature is expected to occur only for hardnesses greater than 234 MPa.

the tip and the measured force does not include the contribution from adhesive forces. The effect of adhesion on plastic indentation is explored by Maugis and Pollock.[49] In our measurements, the measured force is expected to be much greater than adhesive forces except at small indentation depths, so Eq. (6) should be a good approximation.

Using Eqs. (5) and (6) and recalling the definition of the indentation strain rate, we find that, for deformation of the ice by creep,

$$F \approx k(z) v^{1/n}, \tag{7}$$

where $k(z)$ is a function of tip geometry, indentation depth, plastic properties of ice, and temperature. Since $n \geqslant 3$ for polycrystalline ice, we expect that the force required to obtain a given indentation depth at some given temperature should be only weakly dependent on the indentation velocity. As discussed below in Sec. IV D, plastic flow seems to be the dominant indentation mechanism at temperatures below about −15 °C and at large indentation depths.

Figure 8 shows the dependence of the measured hardness on indentation depth at −15 °C, a temperature low enough that plastic flow is expected to dominate. The hardness for several sample speeds is shown for comparison. As the indentation gets deeper, the measured hardness increases, reaching a maximum value that depends on temperature and strain rate if the indentation is deep enough. This is in contrast to the case where the indentation is collected at constant indentation strain rate, where the hardness would be expected to be constant as a function of depth.[42] Because the analysis presented in our earlier paper[29] only considered the hardness at the maximum measured force, it missed the maximum in hardness seen in this figure.

C. Viscous flow of liquid from frictional melting or pressure melting

Frictional melting and pressure melting can both convert solid ice to liquid at the interface while the bulk of the ice remains at a roughly constant temperature well below the melting point. In frictional melting (which generally dominates in skiing[59] and skating[60]), work done by the indenter is converted to heat, raising the temperature of the interface to the melting point of the ice, and providing the latent heat of melting. In our measurements, the work done during the indentation $[W \approx \frac{1}{2}(130\,\text{nm})(1000\,\text{nN}) = 0.065\,\text{pJ}$ from Fig. 3] is less than the latent heat required to melt all of the ice displaced during the process $[W \approx (4.7\times10^{-22}\,\text{m}^3) \times (3.3\times10^{8}\,\text{J/m}^3) = 0.16\,\text{pJ}]$. The heat available from friction for raising the temperature and melting the ice will be significantly less than the work done, since most of the heat will be conducted away before the temperature can be raised to the melting point.[26] Frictional melting can thus be ruled out as the dominant cause of the indentation, but it could shift the local temperature slightly.

In pressure melting, the melting point of the ice is lowered by the large pressures in the ice under the tip. The shift in melting point of the ice is determined by the hydrostatic pressure under the tip. At pressures below those needed for pressure melting, the maximum hydrostatic pressure under the tip is about two-thirds of the measured hardness ($P \approx \frac{2}{3}H$).[52,54] The melting takes heat from its surroundings, cooling them. Because the volume of ice to be melted is small, only a little heat is required (≈0.16 pJ, as shown above). This heat can be provided very rapidly by the slightly warmer tip. If the indentation is done slowly and pressure melting occurs, the pressure under the tip will remain at about the pressure required to shift the melting temperature to the sample temperature as the sample is pressed up against the tip. If the load is increased rapidly, the ice may not flow out of the way quickly enough. In this case pressure will build up, causing more ice to melt. Because the thickness of the melted layer can change during the indentation process, we should not expect the force to be proportional to the velocity, as in the case of QLL flow (described below).

The maximum hardness (see Fig. 8) observed with tips *B* and *C* was sufficient to initiate pressure melting only for the fastest sample velocities at all temperatures studied. The data analyzed with the viscous flow model described in the next section were all obtained under conditions where pressure melting is not expected. Macroscopic indentation hardness measurements on polycrystalline ice by other groups are a factor of 2 or more softer than these maximum hardness values.[53,61,62] Our slowest measurements, in contrast, have much smaller maximum hardness values than the macroscopic measurements. This is believed to be due to viscous flow of the quasiliquid, as discussed below.

D. Viscous flow of interfacial quasiliquid

When the ice-tip, tip-QLL, and QLL-ice interfacial energies are right, the interfacial free energy can be lowered by forming a interfacial melt layer, and quasiliquid forms spontaneously at the interface.[1] Once again, the latent heat required to cause the phase change is rapidly provided by the slightly warmer tip. In contrast to pressure melting, where there is a threshold pressure for melting that depends on the temperature, no pressure is required to form the QLL. As a

TABLE II. Quasiliquid properties from viscous flow model fits. Thickness (h) is calculated assuming the quasiliquid has the viscosity (η) of supercooled water. Uncertainty is estimated from fitting.

	Tip *B*		Tip *C*	
T (°C)	$\frac{h}{\sqrt[3]{\eta}}\left(\frac{\text{nm}}{\sqrt[3]{\text{Pa s}}}\right)$	h (nm)	$\frac{h}{\sqrt[3]{\eta}}\left(\frac{\text{nm}}{\sqrt[3]{\text{Pa s}}}\right)$	h (nm)
−1.01	8.94±1.63	1.10±0.20	5.69±1.22	0.70±0.15
−3.28	3.48±0.55	0.44±0.07	1.90±0.28	0.24±0.04
−5.36	2.62±0.46	0.34±0.06	1.51±0.23	0.20±0.03
−8.28	1.93±0.37	0.26±0.05		
−10.36	1.59±0.25	0.22±0.04		
−10.85			0.93±0.21	0.13±0.03
−13.10	1.46±0.42	0.21±0.06		
−15.10			0.75±0.34	0.11±0.05
−17.24	1.19±0.73	0.18±0.11		

result, only a slight positive pressure is required to push the liquid out of the way and form an indentation. Thus flow of the quasiliquid will continue to enlarge the indentation as long as the tip is pressed into the surface, independent of whether the sample is approaching the tip or being retracted.[32]

To find the relationship between the force on the tip and the indentation depth we must consider the flow of fluid out of the indentation. For a Newtonian fluid which is converted from solid much more rapidly than the indentation process (so that the thickness of the fluid layer is not diminished), force is proportional to velocity for a given indentation depth. As noted in the introduction, the QLL is expected to be near thermal equilibrium since the heat required to form the QLL can be rapidly provided from the environment around the indentation.[26] Assuming additionally that the thickness and viscosity of the fluid are set by the temperature and the chemical and physical properties of the interface (not by pressure or curvature) and that the thickness is small compared to diameter of tip, we show in Appendix A that the parameter that characterizes the indentation is then $h/\eta^{1/3}$, where h is the QLL thickness and η is its viscosity. In particular, Eq. (A4) shows that at a given indentation depth,

$$F \approx \mathcal{F}(z)\left(\frac{h}{\eta^{1/3}}\right)^{-3} v, \tag{8}$$

where $\mathcal{F}(z)$ is a function of tip geometry and indentation depth. Comparing Eq. (7) to (8), it is easy to see that the force is much more strongly dependent on the indentation velocity (v) in the case of viscous flow than it is in the case of plastic flow. Because of this, viscous flow of the QLL is most likely to dominate at small indentation velocities where the force required to move solid ice to the surface is more than the force required for viscous flow. Likewise, viscous flow of the quasiliquid will be most important at temperatures close to the melting point where the QLL will be thickest.

At temperatures above about −11 °C the ratio of force to indentation velocity (F/v) seems to become a universal function of indentation depth that can be fit by our viscous flow model (for at least part of each curve). Below −15 °C the F/v curves at different indentation rates do not collapse onto one curve as well as they do at the higher temperatures, implying that viscous flow is not the dominant indentation mechanism. Using the tip geometry measured for each tip and Eq. (A2), we can find $\mathcal{F}(z)$. The universal portion of the F/v curves can then be fit using Eq. (8) with $h/\eta^{1/3}$ as the single fit parameter. The solid line without point markers in Fig. 5 is the resulting fit for the −5.3 °C data collected with (coated) tip *C*. Table II summarizes the results of fitting the F/v curves at each temperature and for each tip.

Assuming that the QLL has the viscosity of supercooled water, the inferred QLL thickness ranges from 1.1 nm at −1.0 °C to 0.22 nm at −10.4 °C with tip *B*. The same assumption gives us smaller inferred layer thicknesses for tip *C*. In that case, the thickness ranges from 0.70 nm at −1.0 °C to 0.13 nm at −10.9 °C. These values for the thickness are so small that continuum mechanics should not be valid, but our model fits the data quite well. This suggests that the viscosity of the quasiliquid confined between the tip and ice may be greater than that of bulk supercooled water. The uncertainty in the tip geometry results in some uncertainty in the fit parameter. For example, if the end radius of tip *C* were actually 15 nm (as it would be if there were no coating on the end of the tip) the fit of the data collected at −5.3 °C would give $h/\eta^{1/3} \approx 1.24\ \text{nm/(Pa s)}^{1/3}$. This is significantly smaller than the result $h/\eta^{1/3} \approx 1.51\ \text{nm/(Pa s)}^{1/3}$ inferred from a 25 nm end radius. Additionally, the table gives the variation in parameters that fit data from at least two force curves at different acquisition times for a small portion of the curve. Figure 9 gives the viscous layer thickness obtained (with tips *B* and *C*) by assuming that the layer has the viscosity of supercooled water at the appropriate temperature and compares it to other similar studies.

While there is a region of agreement between curves collected at different sample velocities at the higher temperatures, this agreement does not typically occur for the whole curve (see Sec. III A). At small indentations and at large indentations, the force is no longer proportional to the velocity. At small indentations, the precise geometry of the tip end

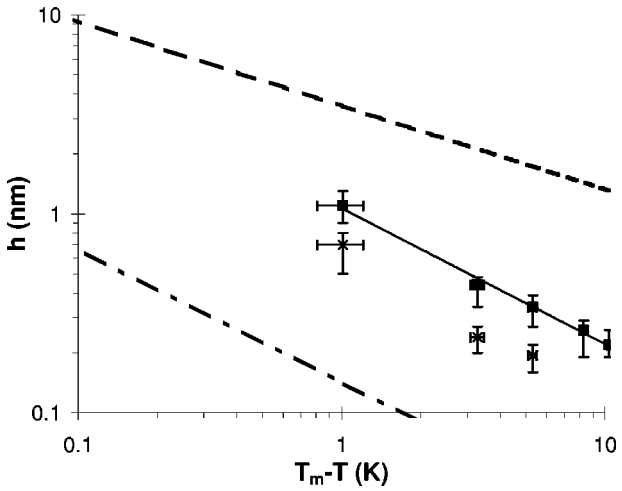

FIG. 9. Interfacial quasiliquid layer thickness as a function of temperature below melting assuming the layer has the viscosity of supercooled water. The upper data points (filled squares) are our measurements for an uncoated silicon tip (*B*) while the lower data points (crosses) are for a hydrophobically coated tip (*C*). Solid line is a fit to the data collected with the uncoated tip [$h \approx 1.1\,\mathrm{nm}(T_m - T)^{-0.68}$, where T is given in Kelvin]. Dashed line is a fit of the thicknesses obtained for ice-metal interfaces from wire regelation experiments (Ref. 12). Dot-dashed line is an extrapolation of results for an ice-polymer interface from flow of the quasiliquid under the influence of a temperature gradient (Ref. 13).

becomes important and the attractive forces between the tip and sample are not negligible. This causes the force/velocity ratio to vary slightly for curves collected at different sample velocities. Since our model assumes a relatively simple tip geometry (a smooth cone with a hemisphere at the end) and does not include internal forces that are not directly measured, it cannot fit the dips that occur because the tip is neither completely smooth nor chemically homogeneous. The F/v data collected with (uncoated) tip *B* (not shown here, but available elsewhere[30]) collapses onto one curve at small indentations and is fit by the simple model much better than that collected with tip *C*. It seems likely that nonuniformities in the coating on tip *C* that produce change in the total force are causing most of the disagreement.

At large indentations, another indentation mechanism seems to become appreciable, decreasing the exponent of the velocity in the force-velocity relation and causing the change in force/velocity ratio with indentation depth to level off. The hardness in many of the curves that exhibit this behavior never reaches values large enough for pressure melting to begin. Plastic flow seems the most likely candidate for this mechanism, but because some viscous flow is still occurring at these indentation depths, the velocity dependence of the indentations is not as simple as in the case of pure plastic flow.

V. CONCLUSIONS

We have measured the indentation behavior of ice at temperatures between $-1\,^{\circ}\mathrm{C}$ and $-17\,^{\circ}\mathrm{C}$. Previous macroscopic hardness measurements of plastic flow in polycrystalline ice found that the hardness was weakly dependent on the loading time, with the hardness proportional to about the one-fourth power of the loading time.[53] Additionally, the macroscopic experiments found that, except at temperatures above about $-3\,^{\circ}\mathrm{C}$, plastic flow of ice under the indenter increased the contact area so that pressure melting did not occur.[53] In our experiments, the curves collected with the largest indentation velocities at temperatures as low as $-17\,^{\circ}\mathrm{C}$ had maximum hardness values sufficient to initiate pressure melting. Our large measured hardness might be due to a grain size larger than the tip contact area for our ice samples.

If the grains are large enough and the bonding between grains is sufficiently strong, our measurements are effectively measurements on single crystals of unknown orientation. Indentation hardness measurements on single crystals often result in hardness values that are much larger than similar measurements on polycrystalline samples.[63] This is partially because, in a polycrystalline sample, the grains can slip against one another, and also partially because some of the grains are oriented so that much of the shear stress on them is in a direction of easy slip, making them easy to deform. In a single crystal indentation experiment the hardness is determined by the stress resolved in the directions of easy slip and is, therefore, sensitive to the orientation of the crystal.[64]

Our hardness measurements at temperatures near the melting point are strongly dependent on indentation velocity suggesting that plastic flow is not the dominant indentation mechanism in our experiments at those temperatures. Viscous flow of a quasiliquid layer between the tip and ice is a mechanism for indentation that provides the observed (proportional) dependence of force on indentation velocity. Using the measured tip shape and a model of this viscous flow, we can estimate the thickness of the QLL if we assume that the viscosity of the layer is that of supercooled bulk water. Layer thicknesses inferred in this way lie between those of previous workers that have studied the QLL at ice solid interfaces using the viscous flow of the quasiliquid (Fig. 9).

It is not surprising that our measurements of the quasiliquid layer thickness do not agree with the previous experiments in Fig. 9. One reason for this is that the (other) solid at the interface in our measurements is different from those used in the other measurements. The QLL thickness is set by the excess interfacial energy which is, in turn, determined by the physical and chemical properties of the materials at the interface (such as the dielectric constant and solubility).[1] Our coated tip (*C*) is probably more similar in chemistry to the polymer film used in the thermally induced flow experiments of Wilen *et al.*[14] than to the metal surfaces of the wires that Gilpin used.[12] The thicknesses inferred from our indentation measurements with both tips have about the same power-law dependence on temperature as the thickness deduced from the thermally induced flow experiments,[13] but the results with tip *C* are about a factor of 5 larger than extrapolated thicknesses from these experiments while those for tip *B* are about a factor of 8 larger. It is important to note that there is no reason that the thickness of the layer deduced from the thermally induced flow experiments must follow our simple extrapolation to thicknesses as small as these, so it is pos-

sible that there is more or less disagreement than we have estimated.

There are several differences between the experiments other than the different solid at the interface that could influence the thickness of the layer. Impurities on the surface of our tip could change the thickness of the QLL in our measurements, by adding electrostatic double-layer forces to the van der Waals forces that are always present. Depending on type and amount of impurities, the thickness of the layer could be enhanced or decreased.[21] Another difference between our experiments and those of Wilen *et al.*[14] is the pressure. The pressures exerted on the ice in our experiment are significantly larger than those in the thermally induced flow experiments. While we have included in our viscous fits only the data where the velocity dependence of the indentation indicates that viscous flow dominates, some plastic flow probably occurs concurrently with the viscous flow. Any plastic flow that occurs concurrently with the viscous flow will reduce the force required to make the indentation, and thereby cause the thickness of the layer that we infer to be overestimated. Additionally, some damage assisted interfacial melting may occur under our tips. This is a nonequilibrium process in which damaged ice is converted to liquid, temporarily enhancing the thickness of the interfacial melt layer.[65] The pressures in our experiments are more comparable to those in the wire regelation experiments, but our thicknesses are at least a factor of 3 less than those of Gilpin and the power-law dependence of his thicknesses on temperature is weaker than ours. This suggests that the different solids and different impurities present in the various experiments could be just as important as the differences in pressure.

The pressure can also shift the melting point of the ice under the tip. Even if there is not enough pressure to cause pressure melting, this can enhance the thickness of the QLL since the thickness is a function of the temperature below melting. Because the pressure near the surface of the ice is near the vapor pressure, this does not affect the ice there. Instead, the thickness of the QLL varies with position along the tip. The curvature of the ice surface also shifts the melting temperature; but because the ice under the tip has negative curvature, the melting point is raised instead of lowered. In our indentation experiments, this effect is small except at very small indentation depths.[30] Neither of the other experiments has enough macroscopic curvature to shift the melting point significantly, but the roughness of the surfaces could cause some local changes in melting point.

The thicknesses given in Fig. 9 were all inferred by assuming that the quasiliquid layer has the viscosity of bulk supercooled water. We will discuss below why we believe that the viscosity of the quasiliquid under our tip is actually significantly greater than that of bulk supercooled water. If this is the case, the actual layer thicknesses in our experiments were larger than those inferred, but we do not know how much larger. The viscosity of the confined QLL varies with temperature, so the power-law relationship between our inferred thicknesses and temperature will not remain the same unless the QLL viscosity is proportional to the viscosity of supercooled bulk water. Assuming that this proportionality occurs, (nonretarded) van der Waals acting alone cannot give us the observed temperature dependence, even in the presence of a shift in melting point due to pressure or curvature. Inclusion of electrostatic double layer forces, as in the DLVO theory, may give the proper temperature dependence.[30]

A. Limitations of viscous model

Our continuum viscous model predicts that the force required to obtain an indentation of a given depth should be proportional to the indentation velocity at which it was collected. In order to simplify our model, we made several assumptions which should be quite reasonable if the quasiliquid layer is thick enough. The assumption that the interfacial melt layer has an abrupt boundary with the solid ice should be valid as long as the QLL is many monolayers thick, since the boundary is expected to be only a few monolayers thick.[66] Recent simulations of the hydrodynamics of very thin layers of Lennard-Jones fluids by Vergeles *et al.*[67] suggest that Stokes's law remains valid even for layers as thin as 5–10 molecular diameters, but the assumption of no slip at the interface may be violated to some extent. Surprisingly, the force in our experiments is observed to be proportional to the velocity for temperatures as low as about $-11\,^{\circ}\mathrm{C}$, where the indentations imply QLL thicknesses of only a single monolayer and our continuum model should fail.

A closer look at the model assumptions shows that most effects that we have left out of the model will decrease the QLL thickness inferred and, therefore, do not help us understand why our model works so well for very small inferred thicknesses. For example, we assumed that the thickness of the QLL is uniform along the tip and is not a function of pressure of the tip. The effect of the variation of QLL thickness with pressure is only important for large indentation velocities and large indentation depths, and will decrease the force required to push the tip into the ice.[30] Decreased force required to obtain an indentation depth at a given indentation velocity in the model results in decreased inferred thickness.

Violation of the no-slip boundary condition at the QLL-ice or QLL-tip boundaries will also decrease the force required to squeeze the quasiliquid from between the tip and the ice. Simulations similar to those of Vergeles *et al.* have shown that there is more slippage at nonwetting fluid-solid interfaces than there is at wetting interfaces.[68] The effect of violation of the no slip boundary condition is that less force is required to obtain an indentation at a given velocity, but we observe the opposite for our hydrophobic tips. Therefore, we do not believe that slippage has a strong influence on our observations.

As mentioned above, plastic flow may act in parallel to the viscous flow to decrease the force required to indent the ice. While plastic flow may be appreciable at the highest speed indentations, it should be negligible at low speeds. Plastic flow, and any other mechanism that acts in parallel to the viscous flow to reduce the force required to indent the ice predicted by the model will decrease the thickness of quasiliquid needed to match our observations.

This leaves two possibilities that can explain ability of our model to fit the observations so well. The first possibility is

that the viscosity of the layer is much greater than the viscosity of supercooled water (so that the layer is thicker than our estimate and Stokes's law remains valid for our data). In order to increase the thickness of the QLL to the level where continuum mechanics should be valid, the viscosity of the quasiliquid would have to increase by at least a factor of three hundred since $h \propto \eta^{1/3}$. This increased viscosity may be due to confinement of the quasiliquid between the tip and the ice, or due to a property of the quasiliquid itself. Significant enhancement of the viscosity of confined liquids has been observed for polymers[69] and, more recently, in water.[70] A second possibility is that there is no significant viscous layer at these interfaces below $-1\,^{\circ}\mathrm{C}$. In this case some other effect must be causing the force to be proportional to the indentation velocity and increasing the (F/v) ratio with indentation depth in such a way our model fits it well using only one parameter. This second possibility seems unlikely, but we cannot rule it out.

B. Effect of tip properties on QLL thickness

Although measurements with both tips result in about the same power-law dependence of thickness on temperature, thickness of the layer at the interface with the coated tip (C) is observed to be thinner than that at the interface with the uncoated tip (B). This was initially surprising to us since we expected the binding between the water molecules and the tip to be weaker at the interface with the hydrophobic coating (tip C), allowing them to be more mobile. A possible explanation for the thicker layer is given by considering the water in the vicinity of a hydrophobic surface above the melting point. In this case, the water molecules reorient themselves so that they can hydrogen-bond to one another, increasing the ordering of the water near the surface over that where hydrogen bonding with the surface is possible.[71] If the QLL behaves this way, some hydrogen bonding with the tip may enhance its thickness.

The van der Waals and electrostatic double-layer interactions may be more important than the hydrophobic effect in determining the layer thickness in our measurements. The Hamaker constant for the silicon-water-ice interface has been calculated by Wilen *et al.* to be about -1.66 zJ,[20] but the Hamaker constant for the coated tip is unknown to us.[72] Additionally, the electrostatic double-layer forces are unknown for both tips since the amount of impurity and surface charge has yet to be quantified. In any case, a quantitative comparison requires knowledge of the viscosity of the quasiliquid.

C. Instabilities

Unlike the measurements of Döppenschmidt *et al.*,[45,48] our results in Fig. 7 show little or no variation in jump-in distance with temperature. There are several possible explanations for our observation. (1) There is no QLL at the ice-vapor interface (since its thickness should have changed with temperature). (2) There is some other force causing the jump-in that has a longer range than the thickness of the layer at the temperatures studied. (3) The sample rate of our instrument is not fast enough to observe the thickness of the layer before the ice under the tip has responded to the presence of the new interface. (4) The tip jumps into the QLL, but comes into mechanical equilibrium in the quasiliquid and does not initially reach the ice surface. Case (4) can be eliminated because we observe the same jump in distances with both tips, and the larger capillary forces from the QLL should give us a larger constant value for the uncoated tip if this were true. Additionally, other experiments[3–8] have shown that there is a QLL at the ice-vapor interface so case (2) or (3) seems most likely.

Our acquisition rates are at least as fast as those of Döppenschmidt *et al.*[45,48] and they measure larger jump-in distances than we do, suggesting that the adhesive forces between their tip and sample pull the tip through any QLL into the ice and begin to deform the ice before they can collect a second data point. This effect is dependent on temperature because the ice is easier to indent at higher temperatures. Our observed increase in indentation depth at zero measured force with temperature given in Fig. 7 shows that the attractive forces between the tip and the sample are large enough to cause indentation even with relatively stiff cantilevers. The main difference between our measurements and those of Döppenschmidt *et al.*[45,48] is that our cantilevers are about a factor of 10 stiffer than theirs. Stiffer cantilevers decrease the force exerted on the sample by the tip-sample adhesive forces immediately following jump-in. Interpretation of jump-in distances as a measure of the thickness of the QLL should be done with caution.

D. Comparison to recent work by Butt *et al.*

After submission of this manuscript, Butt *et al.*[73] published velocity dependent indentation data for ice samples grown from liquid water rapidly frozen on mica and maintained in air at 80% relative humidity. They used silicon nitride cantilevers of approximately two times larger end radius of curvature and 40 times smaller spring constant than the silicon cantilevers used for our tips *B* and *C*. Butt *et al.* assumed that a linear slope for the cantilever deflection versus sample position observed at their highest forces corresponded to the lack of additional tip penetration into the ice. Such an assumption is definitely not satisfied for our data. For example, the data presented in our Fig. 2 indicate linear deflection versus sample position, while the indentation is shown in our Fig. 3 to be increasing throughout the approach curve. Because Butt *et al.* deduced much smaller indentations at their much smaller applied forces, they fit the measured profile of their tips to a parabolic shape. They also assumed a constant attractive capillary force of 30 nN for their data fitting.

Butt *et al.* analyzed their data with a hydrodynamic model similar to that presented by us here and previously,[74] as well as with an extended plastic deformation model that assumed that tip penetration was limited by a ''melting'' rate linearly proportional to the difference between the actual pressure and the yield pressure. (Unfortunately, they were unable to relate the constant of proportionality for the ''melting'' rate of the extended plastic deformation model to any known material property.) By adjusting parameters in their models, they were able to obtain approximate fits to their indentation data at different sample velocities with either model.

Butt *et al.* rejected the hydrodynamic model because the viscosity needed to fit their data was at least 100 times greater than that of supercooled liquid water if an interfacial thickness of one monolayer was assumed. Their values for the mobility parameter $h^3/12\eta$ are appreciably smaller than those deduced from our data. For example, for our tip *B* near $-10\,^{\circ}\mathrm{C}$, our Table II implies $h^3/12\eta = 3.3\times10^{-28}\,\mathrm{m^4s/kg}$, a factor of 36 greater than the value given by Butt *et al.* for their Fig. 10 [assuming their numbers are in $\mathrm{m^4s/kg}$ instead of their stated unit of $\mathrm{m^4/kg\text{-}s}$]. This difference in mobility parameter could be due to the different nature of the silicon-nitride-ice interface and/or to assumptions made in interpreting their measurements.

ACKNOWLEDGMENTS

The authors thank J. Gregory Dash, John S. Wettlaufer, Alan W. Rempel, and Hubert M. Pollock for useful discussions. They also thank NSF DMR 96-23590, University of Washington Nanotechnology Center, and Exxon Educational Foundation for support.

APPENDIX A

As the indentation is formed beneath the tip, some of the ice is displaced to the surface in the form of quasiliquid. Assuming that pressure and curvature at the interface under the tip do not cause the thickness of the layer to vary significantly, and that the ice is converted to quasiliquid much more rapidly than the indentation process, the thickness of the interfacial melt layer between the tip and the ice will be approximately uniform along the tip.[30] Conservation of volume and mass then gives us the average flow velocity in the quasiliquid some distance from the end of the tip. Using this average flow velocity and assuming Newtonian flow with a no-slip condition at the melt-ice and melt-tip boundaries, the Navier-Stokes equation gives the pressure in the liquid as a function of position. The pressure and the flow velocity can then be related to normal and tangential forces on the tip.

The axial symmetry of the problem causes the total force on the tip to cancel except in the *z* direction (parallel to the axis of the tip). Integrating the *z* component of the force per unit area (f_z) from the end of the tip to the region where the ice, vapor, and tip meet, we can obtain the total force on the tip:

$$F = \int_0^{2\pi}\int_0^z f_z(\zeta)g(\zeta)\sqrt{g'^2+1}\,d\zeta\,d\theta$$
$$= 2\pi\int_0^z\left[-\frac{h}{2}\frac{\partial P(\zeta)}{\partial l}+\frac{\eta}{h}v+g'(\zeta)P(\zeta)\right]g(\zeta)\,d\zeta, \tag{A1}$$

where h is the thickness of the quasiliquid layer: η is its viscosity; $g(\zeta)$ is the tip profile given by Eq. (1), $g'(\zeta) \equiv \partial g(\zeta)/\partial\zeta$; l is the distance from the end of the tip along the surface of the tip; z is the indentation depth; v is the indentation velocity; and $P(\zeta)$ is the pressure. This can be broken into a contribution from the drag force on the tip (F_z^d) and from the pressure (F_z^P):[75]

$$F_z^P = -12\pi\frac{\rho_s}{\rho_l}\frac{\eta}{h^3}v\int_0^z d\zeta g(\zeta)g'(\zeta)$$
$$\times\int_z^\zeta d\zeta' g(\zeta')\sqrt{g'(\zeta')^2+1} \tag{A2}$$

and

$$F_z^d = 2\pi\frac{\eta}{h}v\int_0^z d\zeta\left(\frac{3}{h}\frac{\rho_s}{\rho_l}g(\zeta)^2+g(\zeta)\right). \tag{A3}$$

In our experiments, the conditions are such that F_z^d is much less than F_z^P, so a good approximation to Eq. (A1) is given by

$$\frac{F}{v}\approx\frac{F_z^P}{v}=\left(\frac{\eta}{h^3}\right)\mathcal{F}(z), \tag{A4}$$

where $\mathcal{F}(z)$ is a function of tip geometry and indentation depth [see Eq. (A2)].

*Electronic address: fain@phys.washington.edu

[1] J. G. Dash, H. Y. Fu, and J. S. Wettlaufer, Rep. Prog. Phys. **58**, 115 (1995).
[2] V. F. Petrenko and R. W. Whitworth, *Physics of Ice* (Oxford University Press, New York, 1999).
[3] I. Golecki and C. Jaccard, Phys. Lett. A **63**, 374 (1977).
[4] D. Beaglehole and D. Nason, Surf. Sci. **96**, 357 (1980).
[5] Y. Furukawa, M. Yamamoto, and T. Kuroda, J. Cryst. Growth **82**, 665 (1987).
[6] M. Elbaum, S. G. Lipson, and J. G. Dash, J. Cryst. Growth **129**, 491 (1993).
[7] H. Dosch, A. Lied, and J. H. Bilgram, Surf. Sci. **327**, 145 (1995).
[8] H. Dosch, A. Lied, and J. H. Bilgram, Surf. Sci. **366**, 43 (1996).
[9] K. M. Cuffey, H. Conway, B. Hallet, A. M. Gades, and C. F. Raymond, Geophys. Res. Lett. **26**, 751 (1999).
[10] J. J. de Koning, G. de Groot, and G. J. van Ingen Schenau, J. Biomech. **25**, 565 (1992).
[11] I. A. Ryzhkin and V. F. Petrenko, J. Phys. Chem. B **101**, 6267 (1997).
[12] R. R. Gilpin, J. Colloid Interface Sci. **77**, 435 (1980).
[13] J. S. Wettlaufer, M. G. Worster, L. A. Wilen, and J. G. Dash, Phys. Rev. Lett. **76**, 3602 (1996).
[14] L. A. Wilen and J. G. Dash, Phys. Rev. Lett. **74**, 5076 (1995).
[15] T. Ishizaki, M. Maruyama, Y. Furukawa, and J. G. Dash, J. Cryst. Growth **163**, 455 (1996).
[16] M. Elbaum, Ph.D. thesis, University of Washington, 1991.
[17] Y. Furukawa (private communication with S. C. Fain, Jr.), data initially presented [as presented in Ref. 5] in 1987.
[18] H. Dosch (private communication with S. C. Fain, Jr.), data initially presented [as presented in Ref. 7] in 1995.
[19] D. Beaglehole and P. Wilson, J. Phys. Chem. **98**, 8096 (1994).
[20] L. A. Wilen, J. S. Wettlaufer, M. Elbaum, and M. Schick, Phys. Rev. B **52**, 12 426 (1995).
[21] J. S. Wettlaufer, Phys. Rev. Lett. **82**, 2516 (1999).

[22] S. S. Barer, V. I. Kvlividze, A. B. Kurzaev, V. D. Sobolev, and N. V. Churaev, Dokl. Akad. Nauk SSSR **235**, 701 (1977).
[23] S. S. Barer, N. V. Churaev, B. V. Derjaguin, O. A. Kiseleva, and V. D. Sobolev, J. Colloid Interface Sci. **74**, 173 (1980).
[24] N. V. Churaev, S. A. Bardasov, and V. D. Sobolev, Colloids Surf., A **79**, 11 (1993).
[25] P. Barnes, Ph.D. thesis, University of Cambridge, 1968.
[26] V. F. Petrenko, J. Phys. Chem. B **101**, 6276 (1997).
[27] C. R. Slaughterbeck, E. W. Kukes, B. Pittenger, D. J. Cook, P. C. Williams, V. L. Eden, and S. C. Fain, Jr., J. Vac. Sci. Technol. A **14**, 1213 (1996).
[28] C. R. Slaughterbeck, Ph.D. thesis, University of Washington, 1996.
[29] B. Pittenger, D. J. Cook, C. R. Slaughterbeck, and S. C. Fain, Jr., J. Vac. Sci. Technol. A **16**, 1832 (1998).
[30] B. Pittenger, Ph.D. thesis, University of Washington, 2000.
[31] Y.-S. Lo, N. D. Huefner, W. S. Chan, P. Dryden, B. Hagenhoff, and T. P. Beebe, Jr., Langmuir **15**, 6522 (1999).
[32] T. Eastman and D.-M. Zhu, J. Colloid Interface Sci. **172**, 297 (1995).
[33] D. Sarid, *Scanning Force Microscopy* (Oxford University Press, New York, 1991).
[34] The dip in measured force at the beginning of the retract is probably due to frictional forces on the tip which cause a torque at the end of the cantilever. This torque changes sign shortly after the direction of sample motion is changed, causing the measured force to increase slightly. Additionally, there is a slight shift in sample position due to the inability of a quadratic function to perfectly describe the response of the piezo to an applied voltage (Ref. 30).
[35] M. Jaschke and H.-J. Butt, Rev. Sci. Instrum. **66**, 1258 (1995).
[36] D. Tabor, *The Hardness of Metals* (Oxford University Press, London, 1951).
[37] N. P. D'Costa and J. H. Hoh, Rev. Sci. Instrum. **66**, 5096 (1995).
[38] Ultralever batch 006-014 or 017-043. Park Scientific Instruments, 1171 Borregas Ave., Sunnyvale, CA 94089.
[39] J. M. Neumeister and W. A. Ducker, Rev. Sci. Instrum. **65**, 2527 (1994).
[40] R. Luginbuehl, A. Szuchmacher, M. D. Garrison, J.-B. Lhoest, R. M. Overney, and B. D. Ratner, Ultramicroscopy **82**, 314 (2000).
[41] A. W. Adamson, *Physical Chemistry of Surfaces* (Interscience, New York, 1964).
[42] B. N. Lucas, W. C. Oliver, G. M. Pharr, and J.-L. Loubet, in *Thin films: Stresses and Mechanical Properties VI*, edited by W. W. Gerberic, H. Gao, J.-E. Sundgren, and S. P. Baker (Mater. Res. Soc. Symp. Proc. 1997), Vol. 436, pp. 233–238.
[43] A. de Lazeer, M. Dreter, and H. J. Rath, Langmuir **15**, 4551 (1999).
[44] A. W. Rempel (private communication).
[45] A. Döppenschmidt and H.-J. Butt, Langmuir **16**, 6709 (2000).
[46] C. M. Mate, M. R. Lorenz, and V. J. Novotny, J. Chem. Phys. **90**, 7550 (1989).
[47] O. Nickolayev and V. F. Petrenko, in *Evolution of Thin Film and Surface Structure and Morphology*, edited by B. G. Demczyk, E. Garfunkel, B. M. Clemens, E. D. Williams, and J. J. Cuomo (Mater. Res. Soc. Symp. Proc. 1995), Vol. 355, pp. 221–226.
[48] A. Döppenschmidt, M. Kappl, and H.-J. Butt, J. Phys. Chem. B **102**, 7813 (1998).
[49] D. Maugis and H. M. Pollock, Acta Metall. **32**, 1323 (1984).
[50] J. A. King, *Materials Handbook for Hybrid Microelectronics* (Artech House, Boston, 1988).
[51] N. H. Fletcher, *The Chemical Physics of Ice* (Cambridge University Press, London, 1970).
[52] K. L. Johnson, *Contact Mechanics* (Cambridge University Press, Cambridge, 1987).
[53] P. Barnes, D. Tabor, and J. C. F. Walker, Proc. R. Soc. London, Ser. A **324**, 127 (1971).
[54] D. J. Goodman, H. J. Frost, and M. F. Ashby, Philos. Mag. A **43**, 665 (1981).
[55] H. J. Frost and M. F. Ashby, *Deformation-Mechanism Maps: The Plasticity and Creep of Metals and Ceramics* (Pergamon Press, Oxford, 1982).
[56] W. H. Poisl, W. C. Oliver, and B. D. Fabes, J. Mater. Res. **10**, 2024 (1995).
[57] H. M. Pollock, D. Maugis, and M. Barquins, in *Microindentation Techniques in Materials Science and Engineering*, edited by P. J. Blau and B. R. Lawn (American Society for Testing and Materials, Philadelphia, PA, 1986), ASTM STP 889, pp. 47–71.
[58] Equation (6) allows the calculation of the hardness regardless of indentation mechanism, but Eqs. 3 and 5 are only valid for plastic flow.
[59] S. C. Colbeck, J. Sports Sci. **12**, 285 (1994).
[60] S. C. Colbeck, L. Najarian, and H. B. Smith, Am. J. Phys. **65**, 488 (1997).
[61] P. Barnes and D. Tabor, Nature (London) **210**, 878 (1966).
[62] P. Barnes and D. Tabor, in *Commission of Snow and Ice Reports and Discussions* (International Association of Scientific Hydrology, Berne, 1967), Vol. 79, pp. 303–315.
[63] D. Tabor, in *Microindentation Techniques in Materials Science and Engineering*, edited by P. J. Blau and B. R. Lawn (American Society for Testing and Materials, Philadelphia, PA, 1986), ASTM STP 889, pp. 129–159.
[64] J. D. Kiely and J. E. Houston, Phys. Rev. B **57**, 12 588 (1998).
[65] J. G. Dash, B. L. Mason, and J. S. Wettlaufer, J. Geophys. Res. (to be published).
[66] H. Wagner (private communication with J. G. Dash), recent density functional calculations of the lateral shear modulus at the ice-QLL boundary suggest that the boundary is only about three monolayers thick.
[67] M. Vergeles, P. Keblinski, J. Koplik, and J. R. Banavar, Phys. Rev. E **53**, 4852 (1996).
[68] J.-L. Barrat and L. Bocquet, Phys. Rev. Lett. **82**, 4671 (1999).
[69] S. Granick, Science **253**, 1374 (1991).
[70] A. Dhinojwala and S. Granick, J. Am. Chem. Soc. **119**, 241 (1997), a factor of $\approx 10^7$ enhancement in viscosity was observed for a salt (0.1 M of $MgCl_2$) solution confined between mica sheets about 0.6 nm apart. The salt provided a repulsive electrostatic force that overwhelmed the van der Waals attraction and kept the mica surfaces from coming into contact.
[71] J. N. Israelachvili, *Intermolecular and Surface Forces* (Academic Press, New York, 1992).
[72] A rough calculation of the Hamaker constant for a generic hydrocarbon, assuming that all three media have the same absorption frequencies with dielectric constants $\epsilon_w \approx 2.25$, $\epsilon_q \approx 90$, $\epsilon_s \approx 100$ and refractive indices $n_w \approx 1.5$, $n_q \approx 1.333$, $n_s \approx 1.329$ gives $A_{sqw} \approx -0.33$ zJ (Ref. 71). If van der Waals is the only interaction present, the QLL thickness for the coated tip should be about 60% of the value for the uncoated tip. This is about the

right ratio, but the temperature dependence tells us van der Waals is not the only interaction present.

[73] H.-J. Butt, A. Döppenschmidt, G. Hüuttl, E. Müller, and Olga Vinogradova, J. Chem. Phys. **113**, 1194 (2000).

[74] S. Fain, B. Pittenger, M. Cochran, B. Robertson, A. Szuchmacher, and R. Overney, Bull. Am. Phys. Soc. **44-1**, 1383 (1999).

[75] The Couette term was neglected in calculating $P(\zeta)$, but it is instructive to include it to estimate the importance of the motion of the tip relative to the ice.